Final Draft

of the original manuscript

Ivanov, I.; Emurlaev, K.; Lazurenko, D.; Stark, A.; Bataev, I.:

Rearrangements of dislocations during continuous heating of deformed β-TiNb alloy observed by in-situ synchrotron X-ray diffraction.

In: Materials Characterization. Vol. 166 (2020) 110403.

First published online by Elsevier: 29.05.2020

https://dx.doi.org/10.1016/j.matchar.2020.110403

Rearrangements of dislocations during continuous heating of deformed β-TiNb alloy observed by *in-situ* synchrotron X-ray diffraction

Ivan V. Ivanov[a,*], Kemal I. Emurlaev[a], Daria V. Lazurenko[a], Andreas Stark[b], Ivan A. Bataev[a]

[a]*Department of Materials Science and Engineering, Novosibirsk State Technical University, Novosibirsk 630073, Russia*
[b]*Institute of Materials Research, Helmholz-Zentrum Geesthacht, Geesthacht 21502, Germany*

Abstract

Heating of deformed metals always causes changes in their structure and properties. These changes are related to annihilation of the crystallographic defects and rearrangement of the dislocation structure. The currently existing knowledge on structural transformations occurring during the heating of deformed metals is mainly based on *ex-situ* metallographic observation of samples after they have been cooled to room temperature. In this study we attempted to observe defect annihilation and dislocations rearrangement in β-titanium alloy during heating by using *in-situ* synchrotron X-ray diffraction (SXRD). For this reason, a thorough peak profile analysis using *modified* Williamson-Hall (mWH) and *modified* Warren-Averbach (mWA) methods was applied to several hundreds of diffraction patterns obtained during continuous heating of cold rolled Ti45Nb alloy. Several stages of dislocation structure evolution were distinguished based on observation of changes in dislocation density, type of dislocation, energy of dislocations and crystallite size. Such analysis revealed several phenomena which haven't been reported in the literature so far. The results of synchrotron XRD analysis were in excellent agreement with measurements of mechanical properties.

*Correspondence to: Department of Materials Science and Engineering, Novosibirsk State Technical University, 20 Prospekt K. Marksa, Novosibirsk, 630073, Russia.

Email address: i.ivanov@corp.nstu.ru (Ivan V. Ivanov)

Keywords:
Synchrotron X-ray diffraction, *in-situ*, dislocation structure, recovery, polygonization, β-titanium

1. Introduction

It is well known, that heating of cold-worked metals and alloys leads to significant changes in their dislocation structure. The issues of structural changes caused by heat treatment at different temperatures have been studied for a long time. There exists several classifications of the phenomena which occurs due to the heating. Among them the classification based on changes of structure and properties that occur during the annealing of deformed materials is one of the earliest and most well-known. According to this classification, the processes occurring in materials at different temperatures are divided into three main stages: recovery, polygonization and recrystallization [1]. This approach to subdivision is, however, rather conditional, since one stage transforms to another quite smoothly.

The kinetic classification, which implies the separation of stages by elementary mechanisms having different activation energy, seems to be more consistent. According to this classification, the following processes sequentially dominate at different stages of heating: recombination of Frenkel pairs; migration of interstitial atoms to sinks; migration of vacancies to sinks; recombination of screw dislocations; recombination of edge dislocations; formation of subgrains, their growth and rotation; formation of high-angle boundaries and their migration [2].

Optical microscopy, electron microscopy, electron backscatter diffraction (EBSD) and X-ray diffraction (XRD) are the most common methods for studying the processes of structural changes caused by heat treatment [3]. Some indirect methods like ultrasound [4] or calorimetric analyzes [5] are also used for this purpose.

In most of microscopic or diffraction studies the structural changes are evaluated after the heat treatment was already finished and the material is cooled down (i.e. *ex-situ*). However, some of the modern research techniques allow to study structural changes directly during the heating, i.e. *in-situ* (for instance, EBSD [6, 7, 8] or combination of EBSD with scanning electron microscopy (SEM) [9]). The advantage of these methods is the possibility of direct observation of changes in the microstructure of materials. Besides, it allows evaluating the contribution of percipitation and recrystallization separately [9]. As a result, the grain growth kinetics, the change of the individual grain orientation, the material texturing, the energy of low- and high-angle boundaries were studied *in-situ*. However, these methods are mainly used for investigation of transformations on the level of the grain and subgrain structures, but have only limited application on the more fine level associated with structure of crystalline lattice.

To study the structural transformations in materials at the level of individual crystal defects (i.e. point defects, dislocations and dislocation groups) X-ray diffraction in combination with advanced mathematical models are frequently used. For example modified Williamson-Hall (mWH) and modified Warren-Averbach (mWA) methods of peak profile analysis proposed by Ungar [10] can be applied to XRD data. These methods combine the classical Williamson-Hall [11] and Warren-Averbach [12] approaches with dislocation models of strain anisotropy developed by Krivoglaz [13] and Wilkens [14, 15]. Therefore, they allow evaluating such structural parameters of polycrystals as crystallite size, dislocation density, the relative distribution of dislocations by type (or by slip systems), dislocation structure in the material (relative position of dislocations), etc. Several studies have shown that the results obtained using these models are in good agreement with results of transmission electron microscopy (TEM) and consistent with the existing classical concepts [16, 17, 18, 19, 20, 21, 22]. Moreover, previously, these methods were successfully used in *ex-situ* [23] and *in-situ* [24, 25] SXRD experiments. It should be noted that these approaches are currently applicable only to polycrystalline materials of cubic, hexagonal and orthorhombic crystal systems [26].

In this study, mWH and mWA methods were used to analyze the evolution of the dislocation structure of the cold-deformed titanium alloy Ti45Nb during heating. Synchrotron X-ray diffraction (SXRD) measurements were performed using an *in-situ* approach. Ti45Nb is a β-titanium alloy with a single-phase structure possessing a body-centered cubic (BCC) lattice (space group $Im\bar{3}m$), which makes it possible to use the mWH and mWA methods to analyze the structural changes. From the practical point of view this alloy is a promising biomaterial with high corrosion resistance and low Young's modulus [27, 28, 29, 30]. However, the low strength is the significant disadvantage of this alloy [31]. Plastic deformation of Ti45Nb can increase its strength without significant changes in other properties [32]. Finally, β-titanium alloys are used in the aerospace industry due to their high corrosion resistance over a wide temperature range [33, 34]. The use of these materials in jet engine compressors requires an understanding of the changes of their mechanical properties, and, consequently, the dislocation structure during heating to moderate temperatures (up to 770 - 820 K).

2. Experimental procedures

An ingot of Ti45Nb β-titanium alloy was synthesized from technically pure elements in Buehler ArcMelter AM furnace in high purity argon atmosphere. Before the melting, the furnace chamber was triply evacuated to a pressure of $2 \cdot 10^{-8}$ *bar* and flushed with argon. A titanium ingot was used as a getter. The Ti45Nb ingot was remelted 10 times and it was flipped after every second remelting to ensure its chemical homogeneity. The total weight of the ingot was 25 *g*.

The resulting Ti45Nb ingot was cold rolled in several steps. The relative thickness reduction during each rolling step was ~ 8 %. The total thickness reduction was 80 %, so the true strain was 0.59. The specimens for synchrotron X-ray diffraction (SXRD) analysis, microhardness and tension tests were cut out from obtained material using a wire discharge machine.

A size of the specimen used for SXRD experiment was 10 $mm \times 5$ $mm \times 2$ mm. Prior to the experiment the surface of sample was electrochemically polished in an electrolyte consisting of 57 vol. % EtOH, 37 % vol. % i-ProOH and 6 vol. % $HClO_4$. Electropolishing was carried out for 5 minutes at a temperature of 243 K. The surface current density was 20 $mA \cdot cm^{-2}$. After the polishing the surface was cleaned by ethanol and distilled water.

During the diffraction experiment material was heated by the induction method using a modified dilatometer Bähr DIL 805 A/D. The maximum temperature was 1123 K; the heating rate was 293 K/min. To prevent oxidation of the specimen the heating was carried out in an argon atmosphere. S-type thermocouple spot-welded to specimen surface was used to control the temperature.

In-situ SXRD experiment was carried out in transmission mode at the beamline P07 (The High Energy Materials Science) of Deutsches Elektronen-Synchrotron (DESY) operated by Helmholtz-Zentrum Geesthacht. The wavelength of the radiation used during experiment was 0.014 *nm*. The size of the beam was 1 $mm \times 1$ mm. A 16-in. 2D PerkinElmer XRD 1621 scintillation detector with resolution of 127×127 *dpi* was used to record the diffraction patterns. The specimen-to-detector distance was 1.8 *m*.

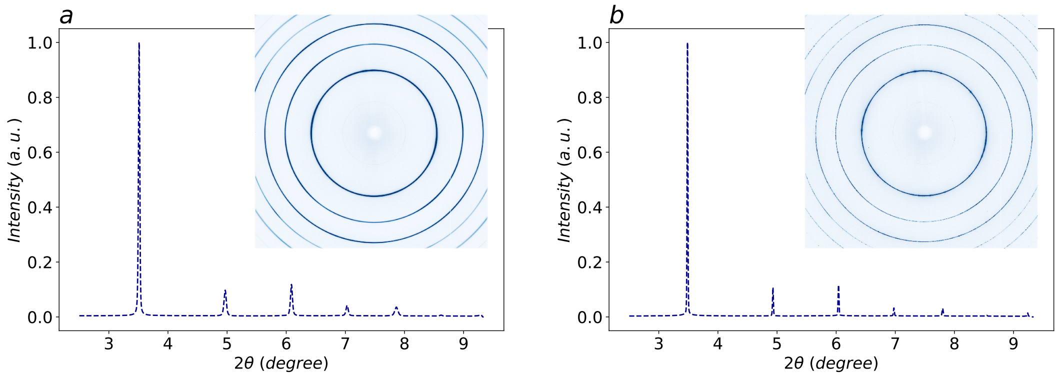

Figure 1: Experimental 2D and azimuthally integrated and normalized 1D diffraction patterns of Ti45Nb in: (a) - as-deformed condition; (b) - heated condition.

Throughout the entire thermal cycle 2D diffraction patterns were recorded at a rate of 6 patterns per minute. The total exposition of each measurement was 4 seconds and it was achieved by summation of 40 frames with exposition time of 0.1 seconds. More than 400 diffraction patterns were recieved during experiment. The obtained diffraction patterns were azimuthally integrated using self-developed Python code based on pyFAI open-source package [35]. Examples of 2D and 1D diffraction patterns are shown in Fig. 1.

Diffraction maxima were fitted using the Pseudo-Voigt function. The instrument-related broadening was estimated by using diffraction pattern of the LaB_6 standard sample. The relationship between full width at half maximum (FWHM) and diffraction angle of the peak was described by the Caglioti function.

Such microstructural characteristics as dislocation density, dislocation type, crystallite size as well as dislocation arrangement were estimated by carefull analysis of the peak profiles using mWH and mWA methods. The theoretical background of these methods is briefly described in Appendix A.

Due to the inevitable increase in the amplitude of phonons oscillations, as well as due to the changes in the elastic properties of the material during its heating several important factors have to be considered prior to application of mWH and mWA methods:

1. The thermal expansion of crystal lattice was derived from the positions of diffraction maxima
2. The influence of thermal vibrations of the crystal lattice was taken into

account using the correction for the dimensionless Debye-Waller factor [36] according to equation:

$$I(\theta) = I_0(\theta)e^{-2M(\theta)} \tag{1}$$

where $I(\theta)$ is the intensity at a given angle θ ; $I_0(\theta)$ is the scattering intensity in the case of a rigid lattice; $M(\theta)$ is the Debye-Waller factor, which can be found as follows:

$$M(\theta) = \frac{6h^2T}{mk_B{\Theta_D}^2}\Big[\phi(x) + \frac{x}{4}\Big]\Big(\frac{sin\theta}{\lambda}\Big)^2 \tag{2}$$

where h is the Planck constant; T is the temperature; m is the mass of the vibrating atom; k_B is the Boltzmann constant; Θ_D is the Debye temperature (542 K for β-titanium [37]); λ is the wavelength; $x = \Theta_D/T$; $\phi(x)$ is the Debye function (the values of which can be found in [36])

To determine the relationship between the structural parameters deduced from SXRD analysis and mechanical properties, the microhardness and the tensile strength of the material were measured. The specimens for mechanical properties were heated in air furnace with precise control of the temperature using the K-type thermocouple and the "Raspberry 3 Model B+" microcontroller. The thermocouple was placed directly under the heated specimen. The specimen was removed from the furnace when the required temperature was reached and cooled down at calm air. The heating rate during the annealing was the same as that during the diffraction experiment. The following heating temperatures were used to prepare the samples for microhardness testing: 298; 373; 473; 573; 673; 698; 748; 798; 823; 873 and 973 K. Also, several specimens heated to temperatures of 298; 723; 773 and 1023 K were used for tensile testing.

The microhardness of materials was measured using a Wolpert Group 402MVD semi-automatic microhardness tester. A tetrahedral diamond pyramid was used as an indenter. The load and the dwell time were 0.98 N and 10 s respectively.

The strength of the specimens was evaluated by uniaxial quasi-static tension using Instron 3369 mechanical testing system. During the tests, the stress-strain curves were recorded and the value of ultimate tensile strength (σ_u) was calculated.

3. Results and Discussion

The main aim of this study was a detailed analysis of changes in dislocation structure during heating of the β-titanium alloy. This problem was addressed by thorough profile analysis of the obtained XRD patterns.

For polycrystalline materials there are two main reasons for broadening of XRD maxima: a decrease in the size of crystallites and an increase in microdistortions of the crystal lattice. These phenomena affect the width of diffraction peaks at different angles in different way. Due to this reason it is possible to deconvolute their influence and quantify their contributions.

The calculations presented in the subsequent sections are based on the Krivoglaz theory of the dislocations effect on the elastic strains of the crystal lattice [13]. The development of this theory led to introduction of several fundamental parameters which are briefly discussed below. The first of them - the dislocation contrast factor $\bar{C}_{hkl}$ - is a "visibility" of dislocations during the experiment. The second parameter denoted in equations proposed by Ungar et. al. as q [38, 10] describes in cubic crystals the distribution of dislocations by their type (edge or screw). More detailed description of these parameters can be found in the Appendix A.

These parameters can be experimentally measured by profile analysis of XRD patterns and calculated theoretically (Eq. A.3). The comparison of the measured and theoretical results allows one to estimate the edge-to-screw dislocations ratio for single-element materials (e.g. copper, iron, nickel). However, in this study, the determination of the parameters $\bar{C}_{hkl}$ and q was associated with a number of difficulties. The reason for this was the lack of precise values of elastic constants c_{11}, c_{12} and c_{44} for Ti45Nb alloy in currently existing literature. Several studies provide both calculated and experimentally determined constants for β-Ti [39, 40, 41]. However, the value of q estimated in this study was beyond the allowed limits for edge and screw dislocations calculated using elastic constants provided in aforementioned studies. Ungar et al [42] faced a similar problem when analyzing the dislocation structure of zirconium hydride. They attributed this fact to the strong anisotropy of the elastic properties of the sample. According to *ab-initio* calculations, in the case of zirconium hydride, the anisotropy parameter A_i may vary in the range from 2 to 7. At the same time, the exact determination of the parameter q requires knowledge of the parameter A_i with precision of better than 1 or 2 units. In addition, the lack of c_{11}, c_{12} and c_{44} values does not allow to estimate the temperature variation of these constants. Due to the above reasons, the quantitative distribution of dislocations by types was not received in this study. However, the qualitative assessment was done based on the variation of the relative value of q.

Despite the disadvantages mentioned above, the combination of several methods of profile analysis is an undoubted advantage of this research. It allowed to study not only the change of the dislocations density, but also the variation of dislocation type, relative position of the dislocations and dynamics of the whole dislocation structure.

The whole picture of changes in the dislocation structure was obtained by simultaneous analysis of several parameters received by mWH and mWA methods:

- ρ - total dislocation density, m^{-2};
- $< x_{area} >$ - area weighted average crystallite size, nm;
- R_e - dislocation outer cut-off radius, nm;
- M - the dimensionless Wilkens parameter, showing the relative position of dislocations: an increase of the parameter indicates a decrease of the stress screening and formation of chaotic dislocation systems; a decrease indicates an increase of the screening and formation of ordered dislocation arrangement;
- q - the dimensionless parameter depending on the type of dislocations in the material: an increase of its value indicates an increase of screw dislocations fraction. And contrary - its decrease indicates an increase in the fraction of edge dislocations.

The results of this study indicate that the process of materials heating is characterized by several distinctive stages, accompanied by significant structural changes (Fig. 2, 3). Three large stages were clearly distinguished - recovery (to 673 K), polygonization (from 673 to 793 K) and subsequent heating phenomena (793 - 1028 K). Moreover, each of these stages is divided into smaller stages:

1. Recovery (298 - 673 K):
    - Stage I (298 - 548 K): slight increase of dislocation density;
    - Stage II (548 - 673 K): annihilation of dislocation dipoles.

2. Polygonization (673 - 793 K):
   - Stage III (673 - 768 K): rapid annihilation of dislocations and growth of crystallite sizes, formation of highly distorted dislocation systems;
   - Stage IV (768-793 K): decrease of the dislocations annihilation rate and growth of crystallite sizes, beginning of dislocation walls formation;
3. Phenomena during the subsequent heating (793 - 1028 K)
   - Stage V (793-853 K): beginning of annihilation of edge dislocations;
   - Stage VI (853-1028 K): low rate of dislocations annihilation, the formation of dislocation walls with a constant velocity, rapid decrease of the fraction of edge dislocations.

In the subsequent sections of this study, each of this stages is described in better detail. The boundaries between key stages are marked with red markers on the plots of parameters derivatives. These stages were distinguished according to specific changes of structural parameters and their temperature derivatives.

3.1. Recovery

The first large stage lasts up to 673 K. In classical literature it is called the recovery stage. At this stage, migration and recombination of point and linear defects occurs, as well as a partial restoration of material's ductility. It is interesting to note, that this stage starts with a slight increase in the dislocation density which was not previously reported. This is clearly seen in Fig. 2b), that shows the change of dislocation density with respect to that of as-rolled sample ($\Delta\rho = \rho - \rho_0$). Moreover, a slight reduction of crystallite size occurs (Fig. 3a). An increase in the density of dislocations occurs up to 548 K. This phenomenon may be expained by the process of point defects diffusion to sinks (e.g. grain or subgrain boundaries, dislocations). As a result a slight increase of the length of dislocation lines occurs. However, the temperature increase also contributes to the formation of new point defects. As a result, the rate of the process will be determined as $V = V^+ + V^-$, where V^+ is the rate of point defects formation; V^- is the rate of point defects diffusion to sinks. The detailed description of the kinetics of these phenomena is presented elsewhere [2, 43].

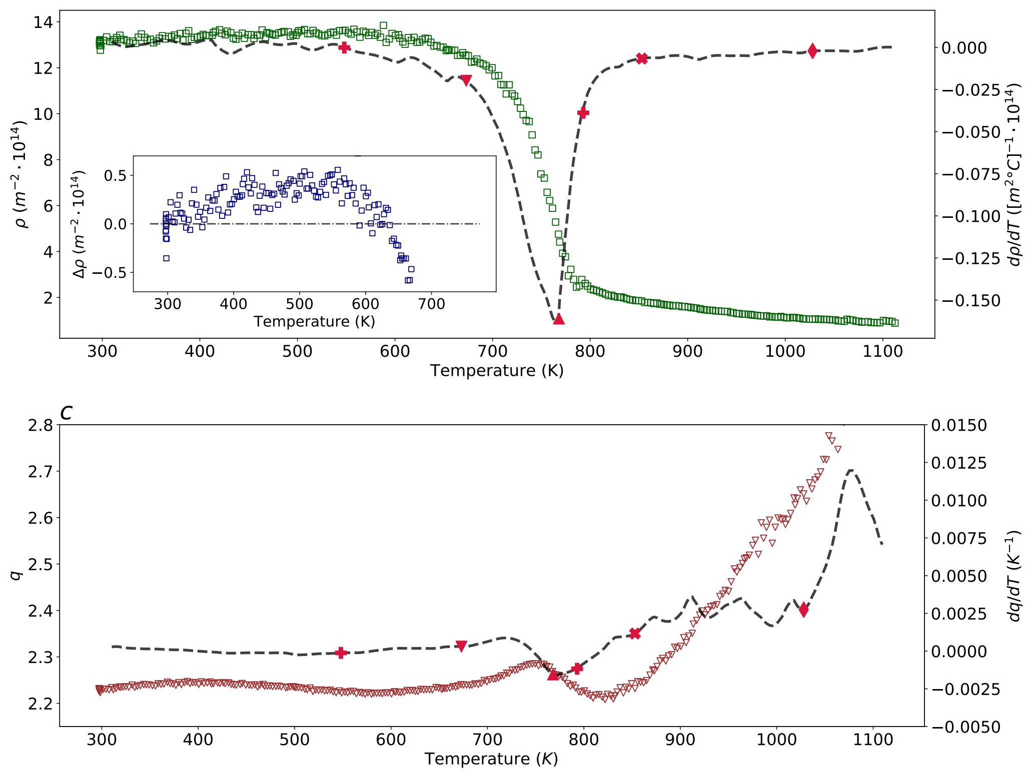

Figure 2: (a) - variation of dislocation density during the heating; (b) - $\Delta\rho = \rho - \rho_0$, where ρ is dislocation density at a certain temperature, ρ_0 is dislocation density in as-deformed state; (c) - temperature variation of parameter q. The dashed lines correspond to the temperature derivatives of the evaluated parameters.

The process of dislocations annihilation starts above 548 K and continues throughout the entire subsequent experiment. Apparently, the initial stage of the annihilation process (i.e. up to 673 K) is a recombination of dislocation dipoles.

From approximately 573 K, a gradual increase of the parameter q starts (Fig. 2c). It indicates that a decrease in the fraction of edge dislocations in the system (i.e. their annihilation) occurs, while the density of screw dislocation doesn't decrease or decreases much slower. This phenomenon is most likely associated with the complex structure of screw dislocations cores in BCC structures. Screw dislocations in BCC structures can form complex sessile dislocation configurations and can dissociate in several non-parallel planes forming highly complex non-planar cores [44]. In the same time, the dissociated edge dislocations in BCC structures have typically planar configuration. Due to this reason edge dislocations in BCC metals are more mobile than screw dislocations, which explains higher rate of their annihilation. Moreover, for BCC metals the limiting process of dislocation movement depends on temperature. For $T < 0.25T_m$ (where T_m is the melting temperature) the limiting process is associated with overcoming the Peierls-Nabarro barrier by dislocations, which occurs by dislocation slip. However, for $T > 0.25T_m$ the limiting processes are the interaction of dislocations with point defects, diffusion and climb [45]. In this way, the annihilation rate of the screw components of the dislocations dipoles in BCC structures is limited by dislocation slip. As a result, only narrow edge dipoles recombine at low temperatures. Subsequent temperature increase enables recombination of wider dipoles of different types [2].

Up to 673 K the recombination rate of both screw and edge dislocations is not significant and does not exceed $-0.025 \cdot 10^{14}(m^2 \cdot K)^{-1}$. In addition, at this stage, there are no significant changes in the $< x_{area} >$ and R_e.

In order to understand the dynamics of R_e (Fig. 3b), it is important to take into account that the stress field of the dislocation structure depends not only on the dislocation density, but also on the relative position of dislocations. If the stress fields of individual dislocations shield each other, the total strain of the crystal lattice decreases with respect to that of non-shielded disordered dislocation arrangement, which leads to a decrease in the value of R_e. Strong stress shielding is a typical characteristic of dislocation dipoles and dislocation walls. The dimensionless Wilkens constant is frequently used to analyze dislocation screening and relative position of dislocations (M). Wilkens constant can be found as $M = R_e\sqrt{\rho}$ [46]. Up to 673 K the value

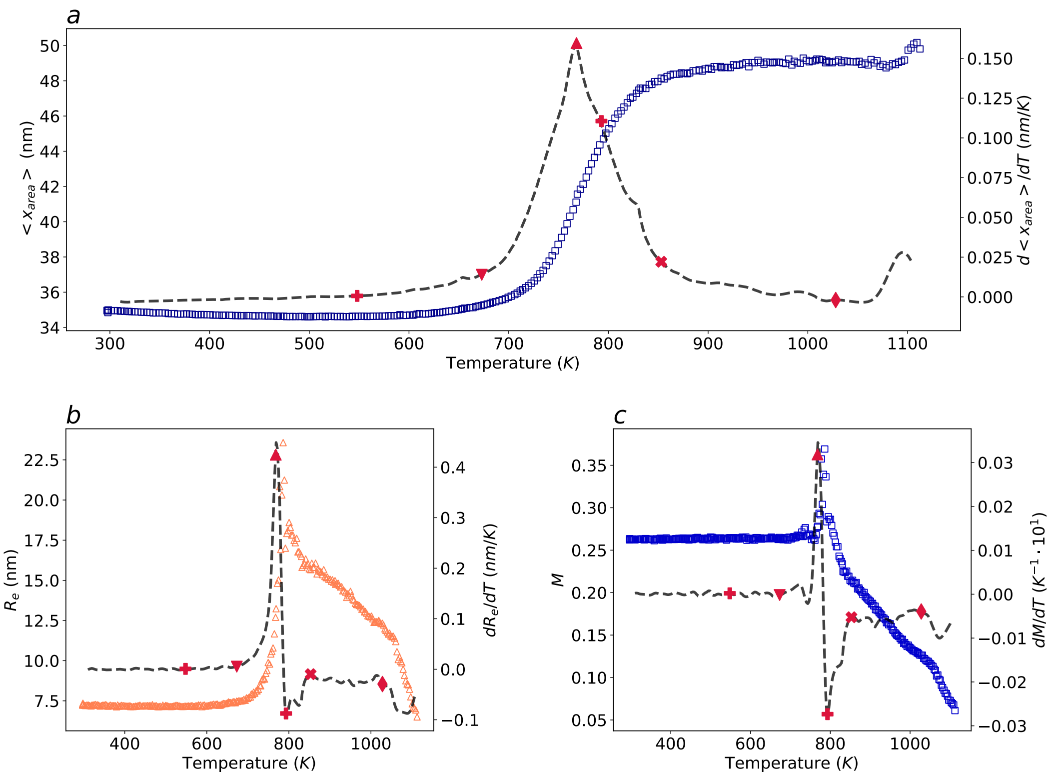

Figure 3: Change of (a) - cristallite size; (b) - dislocation cut-off radius; (c) - Wilkens constant of Ti45Nb during the heating. The dashed lines correspond to the temperature derivatives of the plotted parameters.

of M doesn't change (Fig. 3b,c). It should be noted that dislocation dipole is the most shielded system consisting of two dislocations. Therefore, their recombination should lead only to a slight decrease of the elastic strains of the crystal lattice. Thus, this stage is most likely associated with recombination of dipoles. So the total dislocation density decreases, however, it does not lead to significant changes in the distortion of the crystal lattice and observable changes in R_e and M.

3.2. Polygonization

A further increase of temperature leads to sharp changes in the rate of all parameters. In addition, in the temperature range from 673 to 793 K a sequential increase and decrease of the R_e occurs (Fig. 3b). Firstly, R_e increases from 7.4 to 22 nm in the temperature range 673-768 K. Then it decreases from 22 to 16 nm in the range 773-793 K. This behavior can be explained by considering the interaction energy of dislocations.

This behavior can be explained by considering the interaction energy of dislocations. One of the most descriptive methods of the dislocations interaction energy calculation is based on molecular dynamic simulations. However, this approach requires knowledge of interaction potentials between atoms in the system. Unfortunately, the correct potentials for Ti-Nb system are not available in the literature for Ti45Nb composition. Therefore, to calculate the energy of elastic deformation of a crystal due to interaction of dislocations, a simple model based on the linear theory of elasticity was used in this study. Two dislocations A and B create stresses σ_{ij}^{A} and σ_{ij}^{B} and strains ε_{ij}^{A} and ε_{ij}^{B} in crystal. Then, the energy of a crystal with two dislocations is equal to [47]:

$$E_{strain} = \frac{1}{2}\int_{V} \sigma_{ij}^{\Sigma}\varepsilon_{ij}^{\Sigma} dV \tag{3}$$

According to the superposition principle, the total stress and total strain of the crystal are equal to:

$$\sigma_{ij}^{\Sigma} = \sigma_{ij}^{A} + \sigma_{ij}^{B} \tag{4}$$
$$\varepsilon_{ij}^{\Sigma} = \varepsilon_{ij}^{A} + \varepsilon_{ij}^{B} \tag{5}$$

The energy of the system can be rewritten as follows:

$$E_{strain} = E_{strain}^{A} + E_{strain}^{B} + E_{strain}^{AB} = \frac{1}{2}\int_{V} \sigma_{ij}^{A}\varepsilon_{ij}^{A} dV + \frac{1}{2}\int_{V} \sigma_{ij}^{B}\varepsilon_{ij}^{B} dV + \int_{V} \sigma_{ij}^{AB}\varepsilon_{ij}^{AB} dV \tag{6}$$

where E_{strain}^{A} and E_{strain}^{B} are the energies of dislocations A and B, respectively, and E_{strain}^{AB} is the energy of A and B interaction.

In this study such calculations were done for two dimensional mesh with total size of 200 nm^2. The energy of the system due to the interaction of two parallel edge dislocations of the same sign depending on their relative position is shown on Fig. 4. The first edge dislocation is located in the central position. The position of the second dislocation changed with 0.1 nm step and the Eq. (6) was applied to each of these cases. The values of the energy were normalized by using the maximum value of the energy which is

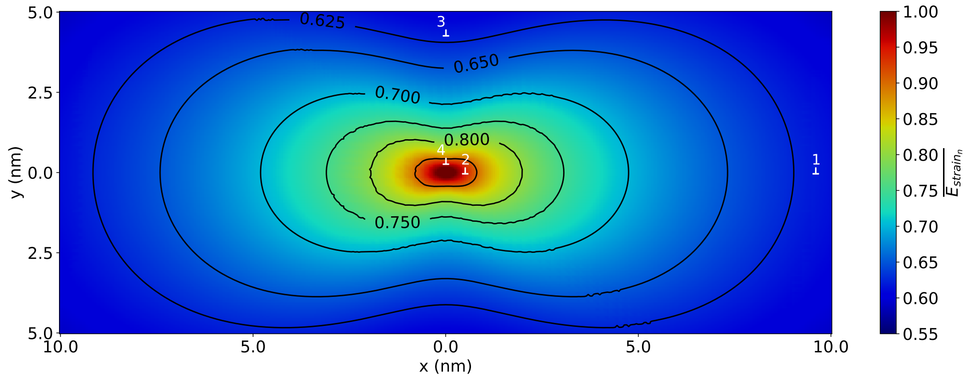

Figure 4: The energy of a crystal depending on the relative position of two positive parallel edge dislocations. Numbered points are indicate the possible positions of first dislocation.

achieved when the distance between two dislocations is twice the core radius [48, 49].

From Fig. 4 it is clear that the most stable configuration of two edge dislocations of the same sign is achieved when one of them is located above or below another. Applying this approach to multiple dislocations will lead to a conclusion, that the lowest energy of the system corresponds to the situation when edge dislocations form a dislocation wall. The average elastic energy due to existence of dislocations in the crystal $< E_{strain} >$ is related to R_e as $< E_{strain} > \approx \ln(R_e/r_0)$, where r_0 is the dislocation core radius. Thus it is proportional to dislocation outer cut-off radius. From here it follows, that the increase of R_e from 7.4 to 22 nm and subsequent decrease from 22 to 16 nm indicates, that $< E_{strain} >$ increases in the range from 673 to 768 K and then rapidly drops down in the range from 768 to 793 K. Thus, the process of dislocation walls formation occurs in two stages.

At the first stage the growth of R_e in the range from 673 to 768 K observed by SXRD experiments and the corresponding growth of $< E_{strain} >$ may be associated with approach of considerable number of dislocations to each other at a distance of several values of the Burgers vector. As an example, it's easy to calculate, that increase of R_e from 7.4 to 22 nm corresponds to 35% of $< E_{strain} >$ growth. This change of energy can be achieved by sliding of one dislocation from the position 1 to 2 during 9 nm, or by climbing from the position 3 to 4 during 4 nm. However, this should mainly occur by dislocation glide, while the dislocation climb at this stage is limited due to its higher activation energy. One may notice, that R_e in temperature range

673-768 K increases with growing rate (Fig. 3b). This can be explained by decreasing of Peierls-Nabarro barriers with temperature. It is known, than dislocation movement through Peierls-Nabarro barriers occurs with the formation of double kinks and their further expansion. However, for dislocations in BCC structures such motion is difficult due to the structural features of their core and an increase of the temperature is required to increase the dislocations mobility. The main reason of this effect is the coherent thermal motion of atoms, and a detailed solution of this problem for the simplest materials in an analytical form is given in [50]. However, in terms of this model the quantitative estimation of the decrease in barrier resistance can be performed only for the simplest systems (e.g. germanium or silicon). The implementation of the solution for complex alloys and for BCC crystals is not possible. Despite this issue, it can be argued that at temperatures well above the Debye temperature, the Peierls-Nabarro barrier decreases with temperature at a rate which is close to exponential. This conclusion is in a good agreement with nearly exponential growth of R_e, observed between 673 and 768 K.

During the next stage (from 768 to 793 K) R_e rapidly decreases to 16 nm (Fig. 3b). This stage is most likely associated with the activation of dislocations climb and the formation of low energy tilt boundaries [3]. In other words, due to the climb phenomenon the dislocations of the same sign move apart from each other, forming stable configurations having lower energy, which explains decrease in Re. I.e. the dislocations occupy positions one above the other as it was discussed for the case of two dislocations shown in Fig. 4. It also can be confirmed by the dynamics of other structural parameters. Firstly, from the 768 K, the growth rate of the parameter q increases. From 793 K a fast and constant growth of this parameter is going on (Fig. 2c). This indicates that from 768 K there is a rapid increase in the fraction of screw dislocations in the system. This stage is also characterized by a decrease in the total dislocation density (Fig. 2a). Therefore, an increase in q can only be associated with the beginning of annihilation of the edge components of dislocations. Secondly, at this stage there is a rapid decrease of the parameter M. This indicates that the shielded dislocation systems, in this case, dislocation walls are formed.

The structural changes described above are part of the polygonization process and they are in very good agreement with the data presented in the classical literature [51]. Polygonization includes the processes of formation, growth, and reorientation of subgrains in crystals containing an excess of dislocations of the same sign.

3.3. Phenomena during the subsequent heating

A subsequent increase in temperature from 793 to 1028 K leads to decrease in the rate of all structural changes. However, the tendency of these processes does not change: there is a gradual decrease of ρ, R_e and M, and increase of $< x_{area} >$. As during the previous stage, dislocations in the specimens are rearranged in the subgrain boundaries.

3.4. Mechanical properties

The correlation of the structural properties of polycrystals and their mechanical properties is a fundamental concept of materials science and dislocation theory of strengthening. The increase in mechanical properties can be achieved by optimizing the number and distribution of defects. This is due to the dual role of the defects. They can both strengthen materials and create prerequisite for their failure [2].

The main features of the fine-grained structure obtained by plastic deformation methods are: the high grain growth rate with increasing temperature; the anisotropy of the structure and properties; the presence of a crystallographic texture; the reduced ductility and deformability. Therefore, heat treatment of plastically deformed materials is often a necessity.

There are several models linking the basic structural parameters and mechanical properties of materials. For homogeneous single-phase materials these models are based on dislocation strengthening theories.

First type of models describes the hardening of materials by the interaction of dislocations. Taylor in 1934 [52] proposed the following equation for growth of the yield strength with the dislocation density increase: $\sigma_{Taylor} = \alpha G b \sqrt{\rho}$, where G is the shear modulus; b is the absolute value of Burgers vector; α is a geometry parameter, depending on the type and relative position of interacting dislocations. For example, the value $\alpha \approx 0.1$ is typical for the interaction of parallel dislocations in one slip system. In the same time, large values are typical for the chaotic dislocation systems [53]. The value of α is usually estimated based on $\sigma - \rho$ curve.

Basinski proposed the modernization of Taylor equation: $\sigma_{Basinsky} = \alpha G b \sqrt{\rho} \ln(1/R_e)$, where $R_e = 1/\rho$ [54]. However, due to the particularities of the dislocation structure of BCC and HCP materials, this model is mainly applicable only for materials with FCC structure.

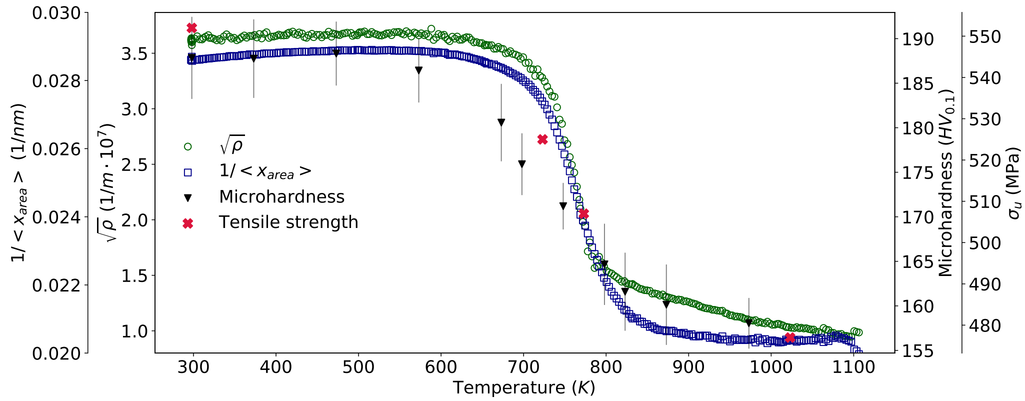

Figure 5: Correlation of dislocation density and crystallite size with microhardness and ultimate tensile strength according to the Kuhlmann-Wilsdorf and Taylor models.

Second type of models links strengthening with the sizes of structural elements of materials. The most common is the Hall-Petch equation: $\sigma_{HP} = Kd^{-0.5}$, where d is an average grain size; K is a constant, which depends on material. According to this model, grain boundaries provide an additional strengthening acting as obstacles to moving dislocations. Since this model operates with sizes of grains (but not with sizes of crystalites, which are measured by XRD analysis) it requires results of microscopic analysis [55].

Besides, there exist models of substructural hardening associated with the subgrain structure. In this case, subgrain walls are considered as dislocations sources. Subgrains contribution to the overall strengthening is determined by their length. According to the Kuhlman-Wilsdorf model, the contribution of subgrains to the yield strength of the material is related to their diameter l as follows: $\sigma_{KW} = k_c l^{-1}$, where k_c is a constant that describes the resistance of subgrain boundary [56]. Therefore, Kuhlmann-Wilsdorf equation was used in this study to describe the correlation between structural changes and mechanical properties. Due to the close correlation between processes occurring during tension and indentation of many metallic materials, these equations are often used to describe the microhardness.

The correlation of crystalline size and dislocation density with mechanical properties according to Taylor and Kuhlmann-Wilsdorf models are shown in Fig. 5.

It can be seen that both ρ and $< x_{area} >$ correlate with the strength and microhardness of materials. One may notice that both parameters have reciprocal dependence on length, besides, it is reasonable to assume that with increase of dislocation density the subgrain size should decrease, which explains the observed correlation. However, according to the equations of Taylor and Kuhlmann-Wilsdorf the influence of these parameters on mechanical properties should be slightly different. Unfortunately, the exact determination of the coefficients α and k_c of the Taylor and Kuhlmann-Wilsdorf equations is very difficult task. This is due to the fact that several competing processes occur during heating, including the reorientation of dislocations and the gradual change of a partially subgrain structure to a grain one. For this reason, the constants α and k_c will also have a functional temperature dependence.

4. Conclusions

In this study SXRD data obtained from continuously heated Ti45Nb specimen were analyzed using mWH and mWA methods to explain the rearrangement of its dislocation structure. Several distinctive stages of structural evolution were observed. In addition to well known stages (i.e. recovery and polygonizatin) several smaller substages can be highlighted.

During the first steps of recovery the slight increase of dislocation density occurs. It can be associated with diffusion of point defects to dislocations as sinks. During the next steps of recovery a slight annihilation of dislocation dipoles and a decrease of dislocation density occurs.

Polygonization stage can be characterized by significant structural changes. Firstly, rapid annihilation of dislocation and growth of crystallite size occurs. Also, this stage is associated with the sharp increase of the energy of the system. It was shown that this phenomena can occur if several dislocations of the same sign come close to each other by slip. The last stages of polygonization in Ti45Nb alloy are associated with slight decrease of dislocation density, increase of the fraction of screw dislocations and formation of dislocation walls by climb of edge dislocations.

Appendix A. Theoretical background of profile analysis methods used in this study

According to the kinematic theory of X-ray diffraction, any diffraction maximum is a result of convolution of the "size" and "distortion" profiles:

$$I^P = I^S \cdot I^D \tag{A.1}$$

where I^P is a "peak" profile; I^S is a "size" profile; I^D is a "distortion" profile.

The approaches to separation of the contribution from these factors to the broadening of diffraction maxima can be divided into convolutional and deconvolutional. Convolutional approaches include, for example, Enzo [57] and Balzar [58] methods. Williamson-Hall (WH) [12] and Warren-Averbach (WA) [11] methods are the most common among deconvolutional approaches. All these approaches have both advantages and disadvantages [59]. Currently, the deconvolutional approaches are the most commonly used for the analysis of the structural parameters of materials. Due to their widespread, these approaches have many modified and refined versions. Two of them, namely the *modified* Williamson-Hall (mWH) and the *modified* Warren-Averbach (mWA) methods, were proposed by Ungar et al [10, 60].

For cubic crystal systems (mWH) equation can be written as follows:

$$\frac{\Delta K^2 - \alpha}{K^2} \backsimeq \beta \overline{C_{h00}}(1 + qH^2) \tag{A.2}$$

where $K = 2\sin\theta/\lambda$ is the reciprocal space coordinate; $\Delta K = \cos\theta \cdot 2\Delta\theta/\lambda$; λ is the wavelength; $2\Delta\theta$ is the full width at half maximum (FWHM); $\alpha = (0.9/D)^2$; $\beta = \pi A^2 b^2 \rho/2$; D is the crystallite size; b is the absolute values of Buergers vector; ρ is the dislocations density; A is a parameter determined by the effective outer cut-off radius of dislocations; $H^2 = (h^2k^2 + h^2l^2 + k^2l^2)/(h^2 + k^2 + l^2)^2$; h, k, l are the Miller indexes of the diffraction maximum.

Parameters $\overline{C_{h00}}$ and q should be found experimentally and compared with theoretical values. Theoretical values of these parameters for cubic materials possess the following functional relationship:

$$f(A_i, c_{12}, c_{44}) = a(c_{12}, c_{44})\big[1 - exp\big(-A_i/b(c_{12}, c_{44})\big)\big] + c(c_{12}, c_{44})A_i + d(c_{12}, c_{44}) \tag{A.3}$$

where c_{11}, c_{12}, c_{44} are the elastic constants of material; $A_i = 2c_{44}/(c_{11} - c_{12})$ is the anisotropy parameter; $a(c_{12}, c_{44})$, $b(c_{12}, c_{44})$, $c(c_{12}, c_{44})$, $d(c_{12}, c_{44})$ are the parameters which depend on c_{12}/c_{44} ratio.

The values of these parameters for some materials and detailed description of functional relationships can be found elsewhere [38].

The mWA equation has the following form:

$$\ln A(L) = \ln A^S(L) - \frac{\pi\rho}{2} \cdot L^2 \ln(\frac{R_e}{L})(\overline{g^2 C_{hkl} b^2}) + O \cdot (\overline{g^2 C_{hkl} b^2})^2 \quad \text{(A.4)}$$

where g is the diffraction vector ($g = K$ at the exact Bragg position); L is the Fourier length [the distance between two lattice points in the ideal average crystal which are aligned normal to the planes (hkl)] defined as $L = na_3$ (where $n \in Z$); $a_3 = \frac{\lambda}{2(\sin(\theta_2)-\sin(\theta_1))}$ is the unit of the Fourier length in the direction of the diffraction vector g; $\overline{C_{hkl}}$ is the average dislocation contrast factor; R_e is the dislocation outer cut-off radius.

Approximation of mWA Eq. A.4 by quadratic equation $y = S+Yz+Oz^2$, where $y = lnA(L)$; $z = \overline{g^2 C_{hkl} b^2}$ allows one to obtain two coefficients that are required for subsequent calculations. The coefficients S and Y describe size and distortion contributions, respectively.

Langford and Wilson [61] showed that for spherical particles, the mean squared crystallite size is proportional to the parameter L_0 ; that is, to the value of L, when $A(L) = 0$. To find the average crystallite size, one has to approximate the initial values of the size Fourier coefficients by a linear function.

In turn, the values obtained for the coefficient Y can be written using the following functional relationship:

$$\frac{Y}{L^2} = \rho\frac{\pi}{2} \ln R_e - \rho\frac{\pi}{2} \ln L \quad \text{(A.5)}$$

Linearization of this relationship allows us to obtain the ρ and R_e.

Acknowledgments

This study was partially supported by The Ministry of Education and Science of Russian Federeation (project "Analysis of metastable structures at material interfaces during extreme external impacts").

References

[1] S. S. Gorelik, Recrystallization in metals and alloys.[in russian], MIR Publishers, 1981, (1981) 479.

[2] L. N. Larikov, Healing of defects in metals [in russian], Kiev, Naukova dumka (1980).

[3] F. J. Humphreys, M. Hatherly, Recrystallization and related annealing phenomena, Elsevier, 2012.

[4] P. Palanichamy, M. Vasudevan, T. Jayakumar, S. Venugopal, B. Raj, Ultrasonic velocity measurements for characterizing the annealing behaviour of cold worked austenitic stainless steel, NDT & E International 33 (2000) 253–259.

[5] G. Benchabane, Z. Boumerzoug, I. Thibon, T. Gloriant, Recrystallization of pure copper investigated by calorimetry and microhardness, Materials characterization 59 (2008) 1425–1428.

[6] A. Chakkedath, D. Hernández-Escobar, C. J. Boehlert, In-situ observations of recrystallization and microstructural evolution in cerium-containing rolled magnesium alloys, International Journal of Lightweight Materials and Manufacture 1 (2018) 256–264.

[7] F. Brisset, A.-L. Helbert, T. Baudin, In situ electron backscatter diffraction investigation of recrystallization in a copper wire, Microscopy and Microanalysis 19 (2013) 969–977.

[8] A.-L. Helbert, W. Wang, F. Brisset, T. Baudin, R. Penelle, In situ ebsd investigation of recrystallization in a partially annealed and cold-rolled aluminum alloy of commercial purity, Advanced Engineering Materials 14 (2012) 39–44.

[9] J. Tändl, S. Nambu, A. Orthacker, G. Kothleitner, J. Inoue, T. Koseki, C. Poletti, In-situ observation of recrystallization in an almgsczr alloy using confocal laser scanning microscopy, Materials characterization 108 (2015) 137–144.

[10] T. Ungár, A. Borbély, The effect of dislocation contrast on x-ray line broadening: A new approach to line profile analysis, Applied Physics Letters 69 (1996) 3173–3175.

[11] B. Warren, B. Averbach, The effect of cold-work distortion on x-ray patterns, Journal of applied physics 21 (1950) 595–599.

[12] G. Williamson, W. Hall, X-ray line broadening from filed aluminium and wolfram, Acta metallurgica 1 (1953) 22–31.

[13] M. A. Krivoglaz, Theory of X-Ray and Thermal Neutron Scattering by Real Crystals, Plenum Press, 1969.

[14] M. Wilkens, The determination of density and distribution of dislocations in deformed single crystals from broadened x-ray diffraction profiles, Physica status solidi (a) 2 (1970) 359–370.

[15] M. Wilkens, Theoretical aspects of kinematical x-ray diffraction profiles from crystals containing dislocation distributions(fourier transform of x ray diffraction line profiles from crystals with dislocations), NBS Fundamental Aspects of Dislocation Theory 2 (1970).

[16] N. Forouzanmehr, M. Nili-Ahmadabadi, M. Bönisch, The analysis of severely deformed pure Fe structure aided by X-ray diffraction profile, The Physics of Metals and Metallography 117 (2016) 624–633. URL: `http://link.springer.com/10.1134/S0031918X16060077`. doi:`10.1134/S0031918X16060077`.

[17] R. Valiev, R. S. Musalimov, High-resolution transmission electron microscopy of nanocrystalline materials, Physics of Metals and Metallography 78 (1994) 666–670.

[18] R. Valiev, Nanostructuring of metals by severe plastic deformation for advanced properties, Nature materials 3 (2004) 511.

[19] I. Dragomir, T. Ungár, Contrast factors of dislocations in the hexagonal crystal system, Journal of Applied Crystallography 35 (2002) 556–564.

[20] J. Gubicza, I. C. Dragomir, G. Ribárik, Y. T. Zhu, R. Valiev, T. Ungár, Characterization of the microstructure of severely deformed titanium by x-ray diffraction profile analysis, in: Materials Science Forum, volume 414, Trans Tech Publ, 2003, pp. 229–234.

[21] V. Stolyarov, Y. Zhu, T. Lowe, R. Islamgaliev, R. Valiev, A two step spd processing of ultrafine-grained titanium, Nanostructured Materials 11 (1999) 947–954.

[22] V. V. Stolyarov, Y. T. Zhu, I. V. Alexandrov, T. C. Lowe, R. Z. Valiev, Influence of ecap routes on the microstructure and properties of pure ti, Materials Science and Engineering: A 299 (2001) 59–67.

[23] I. V. Ivanov, D. V. Lazurenko, A. Stark, F. Pyczak, A. Thömmes, I. A. Bataev, Application of Different Diffraction Peak Profile Analysis Methods to Study the Structure Evolution of Cold-Rolled Hexagonal α-Titanium, Metals and Materials International (2019). URL: http://link.springer.com/10.1007/s12540-019-00309-z. doi:10.1007/s12540-019-00309-z.

[24] N. Sallez, X. Boulnat, A. Borbély, J. L. Béchade, D. Fabrègue, M. Perez, Y. De Carlan, L. Hennet, C. Mocuta, D. Thiaudière, Y. Bréchet, In situ characterization of microstructural instabilities: Recovery, recrystallization and abnormal growth in nanoreinforced steel powder, Acta Materialia 87 (2015) 377–389. doi:10.1016/j.actamat.2014.11.051.

[25] M. Kerber, F. Spieckermann, R. Schuster, B. Joni, N. Schell, E. Schafler, In-situ synchrotron profile analysis after high-pressure torsion deformation, Crystals 9 (2019) 1–12. doi:10.3390/cryst9050232.

[26] G. Ribárik, Modeling of Diffraction Patterns Based on Microstructural Properties: Ph. D. Thesis, Ph.D. thesis, 2008.

[27] R. Godley, D. Starosvetsky, I. Gotman, Corrosion behavior of a low modulus β-Ti-45 % Nb alloy for use in medical implants, Journal of Materials Scince in Medicine 17 (2006) 63–67. doi:10.1007/s10856-006-6330-6.

[28] P. F. Gostin, A. Helth, A. Voss, R. Sueptitz, M. Calin, J. Eckert, A. Gebert, Surface treatment, corrosion behavior, and apatite-forming ability of ti-45Nb implant alloy, Journal of Biomedical Materials Research - Part B Applied Biomaterials 101 B (2013) 269–278. doi:10.1002/jbm.b.32836.

[29] G. Zorn, I. Gotman, E. Y. Gutmanas, R. Adadi, G. Salitra, C. N. Sukenik, Surface modification of Ti45Nb alloy with an alkylphosphonic acid self-assembled monolayer, Chemistry of Materials 17 (2005) 4218–4226. doi:10.1021/cm050477f.

[30] G. Zorn, A. Lesman, I. Gotman, Oxide formation on low modulus Ti45Nb alloy by anodic versus thermal oxidation, Surface and Coatings Technology 201 (2006) 612–618. doi:10.1016/j.surfcoat.2005.12.009.

[31] K. Ozaltin, W. Chrominski, M. Kulczyk, A. Panigrahi, J. Horky, M. Zehetbauer, M. Lewandowska, Enhancement of mechanical properties of biocompatible ti–45nb alloy by hydrostatic extrusion, Journal of Materials Science 49 (2014) 6930–6936.

[32] B. Völker, N. Jäger, M. Calin, M. Zehetbauer, J. Eckert, A. Hohenwarter, Influence of testing orientation on mechanical properties of ti45nb deformed by high pressure torsion, Materials & Design 114 (2017) 40–46.

[33] R. Boyer, Titanium for aerospace: Rationale and applications, Advanced Performance Materials 2 (1995) 349–368.

[34] R. Boyer, R. Briggs, The use of β titanium alloys in the aerospace industry, Journal of Materials Engineering and Performance 14 (2005) 681–685.

[35] G. Ashiotis, A. Deschildre, Z. Nawaz, J. P. Wright, D. Karkoulis, F. E. Picca, J. Kieffer, The fast azimuthal integration python library: pyfai, Journal of applied crystallography 48 (2015) 510–519.

[36] B. Cullity, S. Stock, Elements of X-ray Diffraction, Third Edition, Prentice-Hall, 2001.

[37] Q. Chen, B. Sundman, Calculation of debye temperature for crystalline structures—a case study on Ti, Zr, and Hf, Acta Materialia 49 (2001) 947–961. URL: https://linkinghub.elsevier.com/retrieve/pii/S1359645401000027. doi:10.1016/S1359-6454(01)00002-7.

[38] T. Ungár, I. Dragomir, Á. Révész, A. Borbély, The contrast factors of dislocations in cubic crystals: The dislocation model of strain anisotropy in practice, Journal of Applied Crystallography 32 (1999) 992–1002. doi:10.1107/S0021889899009334.

[39] J. Nejezchlebová, M. Janovská, P. Sedlák, J. Šmilauerová, J. Stráský, M. Janeček, H. Seiner, Elastic constants of β-Ti15Mo, Journal of

Alloys and Compounds 792 (2019) 960–967. doi:10.1016/j.jallcom.2019.03.418.

[40] H. Ledbetter, H. Ogi, S. Kai, S. Kim, M. Hirao, Elastic constants of body-centered-cubic titanium monocrystals, Journal of applied physics 95 (2004) 4642–4644.

[41] Q. Chen, L. Liu, C. Zhu, K. Chen, Mesomechanical modeling and numerical simulation of the diffraction elastic constants for ti6al4v polycrystalline alloy, Metals 8 (2018) 822.

[42] T. Ungar, Quantification of dislocations densities in zirconium hydride by X-ray line profile analysis, Acta Materialia 117 (2016) 1–12. doi:10.1016/j.actamat.2016.06.058.

[43] R. W. Balluffi, D. N. Seidman, Annealing kinetics of vacancies to dislocations, Philosophical Magazine 17 (1968) 843–848. doi:10.1080/14786436808223033.

[44] N. Noskova, Defects and Deformation of Single Crystals, Ekaterinburg, UB RAS, 1995.

[45] H. Conrad, Thermally activated deformation of metals, JOM 16 (1964) 582–588.

[46] J. Gubicza, X-Ray Line Profile Analysis in Materials Science, 2014. URL: http://services.igi-global.com/resolvedoi/resolve.aspx?doi=10.4018/978-1-4666-5852-3. doi:10.4018/978-1-4666-5852-3.

[47] A. Predvoditelev, N. Tyapunina, G. Zinenkova, G. Bushueva, Physics of crystals with defects [In Russian], MSU Press, Moscow, 1986.

[48] R. Chang, L. J. Graham, Edge Dislocation Core Structure and the Peierls Barrier in Body-Centered Cubic Iron 99 (1966) 99–103.

[49] G. Monnet, D. Terentyev, Structure and mobility of the $1/2 < 111 >$ $\{112\}$ edge dislocation in BCC iron studied by molecular dynamics, Acta Materialia 57 (2009) 1416–1426. URL: http://dx.doi.org/10.1016/j.actamat.2008.11.030. doi:10.1016/j.actamat.2008.11.030.

[50] J. Friedel, Dislocations: International Series of Monographs on Solid State Physics, volume 3, Elsevier, 2013.

[51] L. Larikov, Physical Principles of Strength and Plasticity of Metals [In Russian], Metallurgizdat, Moscow, 1963.

[52] G. I. Taylor, The mechanism of plastic deformation of crystals. part i.—theoretical, Proceedings of the Royal Society of London. Series A, Containing Papers of a Mathematical and Physical Character 145 (1934) 362–387.

[53] H. Mughrabi, The α-factor in the taylor flow-stress law in monotonic, cyclic and quasi-stationary deformations: Dependence on slip mode, dislocation arrangement and density, Current Opinion in Solid State and Materials Science 20 (2016) 411 – 420. URL: `http://www.sciencedirect.com/science/article/pii/S1359028616300870`. doi:`https://doi.org/10.1016/j.cossms.2016.07.001`, the COSSMS Twentieth Anniversary Issue.

[54] Z. Basinski, Forest hardening in face centred cubic metals, Scripta Metallurgica 8 (1974) 1301–1307.

[55] Z. Zhang, S. Qu, A. Feng, J. Shen, Achieving grain refinement and enhanced mechanical properties in ti–6al–4v alloy produced by multidirectional isothermal forging, Materials Science and Engineering: A 692 (2017) 127–138.

[56] B. B. M.I. Goldstein, V.S. Litvinov, Metallophysics of high-strength alloys [In Russian], Metallurgy, Moscow, 1986.

[57] S. Enzo, G. Fagherazzi, A. Benedetti, S. Polizzi, A profile-fitting procedure for analysis of broadened x-ray diffraction peaks. i. methodology, Journal of Applied Crystallography 21 (1988) 536–542.

[58] D. Balzar, Diffraction Line Broadening - Nuisance or Lattice-Imperfections Fingerprints, Croatica Chemica Acta 69 (1996) 1069–1115.

[59] B. Marinkovic, R. R. de Avillez, A. Saavedra, F. C. R. Assunção, A comparison between the Warren-Averbach method and alternate

methods for X-ray diffraction microstructure analysis of polycrystalline specimens, Materials Research 4 (2001) 71–76. doi:10.1590/s1516-14392001000200005.

[60] I. C. Dragomir, T. Ungár, Contrast factors of dislocations in the hexagonal crystal system, Journal of Applied Crystallography 35 (2002) 556–564. doi:10.1107/S0021889802009536.

[61] J. I. Langford, A. Wilson, Scherrer after sixty years: a survey and some new results in the determination of crystallite size, Journal of applied crystallography 11 (1978) 102–113.